Closed-Loop Compensation of Kinematic Error in Harmonic Drives for Precision Control Applications

Prasanna S. Gandhi, *Associate Member, IEEE,* and Fathi H. Ghorbel, *Senior Member, IEEE*

***Abstract*—In this paper, we present nonlinear control algorithms to compensate for kinematic error in harmonic drives, thus forming a solid basis to improve their performance in precision positioning applications. Kinematic error, defined as deviation between expected and actual output positions, influences performance by producing static positioning error and inducing dynamic vibration effects. Its compensation is difficult because of its nonlinear behavior and dependence on drive type, assembly, environmental conditions, and drive load. The Lyapunov-based closed-loop control algorithms presented in this paper compensate for the kinematic error irrespective of its form in setpoint and trajectory tracking applications (Rice University patent pending). Simulation and experimental results obtained with a dedicated harmonic drive test setup verify the effectiveness of the proposed controllers.**

***Index Terms*—Harmonic drives, kinematic error, Lyapunov stability, regulation, tracking.**

I. Introduction

HARMONIC drives are special flexible gear transmission systems. Their typical construction with meshing at two diametrically opposite ends gives them many useful properties. These include compact design with low weight, high gear reduction with almost zero backlash, and high torque-to-weight ratio. Hence, these drives are popular in many precision positioning applications such as wafer handling and laser mirror positioning machines in the semiconductor industry, lens grinding machines, and precision measuring devices [1]. They are also ideal for space robots and satellite actuators due to their high torque-to-weight ratio which enables them to be directly mounted at robot joints. Additionally, they are widely used in tracking devices for military and commercial applications. Harmonic drives are making headway in industrial as well as military and space applications.

A harmonic drive is composed of the components identified in Fig. 1(a). The wave generator is a rigid steel core having an elliptical shape with very small eccentricity. It is surrounded by a flexible race ball bearing. The flexible spline (or flexspline) is a thin-walled hollow cup made up of alloy steel. External gear teeth are machined at the open end of this cup and the closed end is connected to the output shaft. The circular spline is a rigid internal gear having two teeth more than those on the flexspline. Upon assembly, the wave generator fits into the open end of the flexspline cup and gives it an elliptical shape at that end. The circular spline teeth then mesh with the flexspline teeth at the major axis of the ellipse defined by the wave generator. A fully assembled harmonic drive is shown in Fig. 1(b). In the most common speed reduction configuration, the wave generator serves as the input port, the flexspline acts as the output port, and the circular spline is held immobile.

The concept of harmonic drives was conceived and developed during the mid-1950s [3], [4]. Their industrial use for different applications has been growing since then. However, research in the theoretical aspects of their transmission characteristics has not been extensive. Most of the work in this area has been carried out in nonlinear transmission attributes including kinematic error, flexibility, and hysteresis [5]–[12], and in design attributes including tooth stresses and geometry [13]–[15].

Of the different transmission attributes mentioned above, kinematic error is of foremost concern for precision positioning applications. Kinematic error $\tilde{\theta}$ is defined as the deviation between the expected output position and the actual output position. It is given by the following equation (see Fig. 2):

$$\tilde{\theta} = \frac{\theta_m}{N} - \theta_l \tag{1}$$

where θ_m is the rotation of the motor shaft attached to the wave generator, N is the gear reduction ratio, and θ_l is the rotation of the output shaft connected to the flexspline or the circular spline as the case may be. The experimental kinematic error waveforms presented in the literature [9], [12] show small magnitude with periodic nature; for instance, the waveform reported in [12] (see Fig. 2) is periodic with magnitude of 0.05°. Also, the fundamental frequency of these waveforms is reported to be twice the frequency of wave generator rotation. In addition to the fundamental, small high-frequency error components are observed. Besides producing a static error in load position, kinematic error acts as a periodic exciter and causes undesirable vibration effects. These vibrations serve as an energy sink and produce dramatic torque losses and velocity fluctuations [9]. Thus, kinematic error has both static and dynamic effects which lead to performance degradation in precision regulation and tracking. Hence, compensation of kinematic error is of utmost importance for precision positioning with harmonic drives.

Properties of kinematic error and causes of its occurrence have been studied in the past by several researchers [5]–[8], [16]. It is only recently that we completely characterized kinematic error in [12] where we found that it differs for different

Manuscript received July 13, 2000. Manuscript received in final form March 13, 2002. Recommended by Associate Editor L. K. Mestha. This work was supported in part by the National Science Foundation under Grant INT-9819869 and by the Texas Advanced Technology Research Program under Grant TATP 003604-057.

P. S. Gandhi is with the Department of Mechanical Engineering, Indian Institute of Technology, Bombay 400076, India (e-mail: gandhi@me.iitb.ac.in).

F. H. Ghorbel is with the Department of Mechanical Engineering, Rice University, Houston, TX 77005 USA (e-mail: ghorbel@rice.edu).

Digital Object Identifier 10.1109/TCST.2002.804119

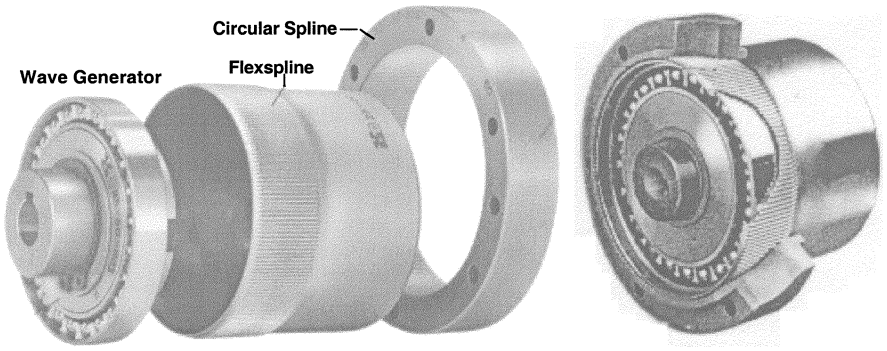

Fig. 1. (a) Harmonic drive gear components and (b) assembly [1].

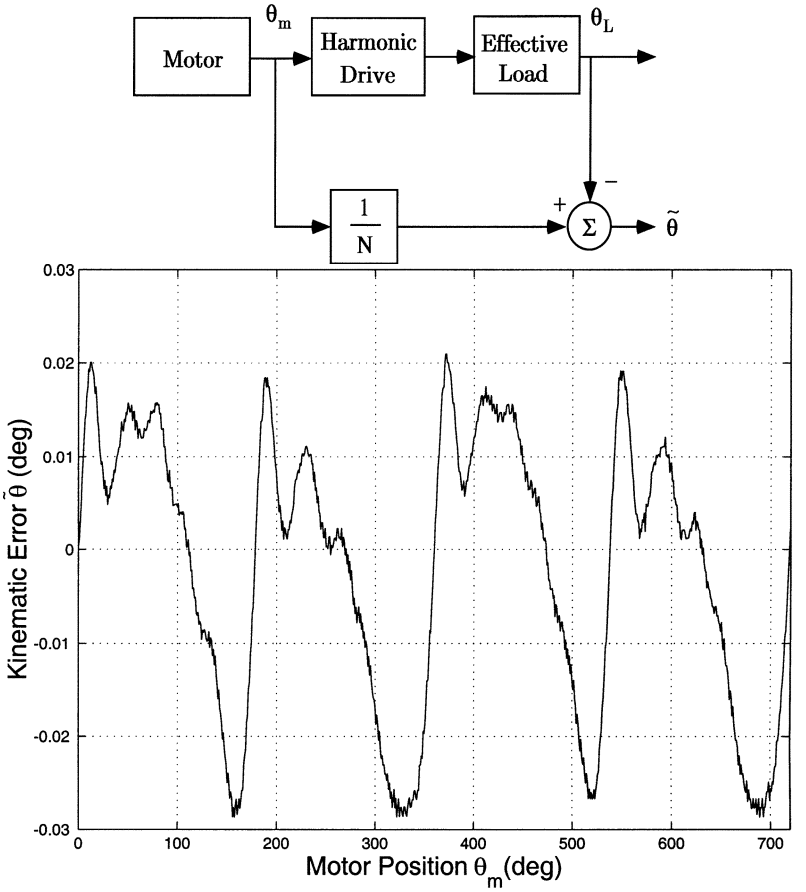

Fig. 2. Typical experimental waveform of kinematic error.

drives, speeds, assemblies, and loading conditions. In particular, we reported in [12] that as motor speed is increased, kinematic error waveform gets colored by flexibility effects. Hence, the concept of "pure form" of kinematic error was introduced for the first time in [12]. The pure form, defined at a low speed, goes on varying as the load on output shaft is increased. Also, the pure form changes with variations in assembly conditions. The sensitivity of kinematic error to assembly, load, and speed as we reported in [12] explained the variability of the experimental error waveforms that appear in the literature [8], [16], [12]. In addition, kinematic error was reported to be sensitive to environmental conditions [8], [12]. Thus, compensation of this nonlinear, operating condition-dependent, drive-specific kinematic error poses a challenging task.

To the best of our knowledge, the complete compensation of kinematic error in setpoint and trajectory tracking with harmonic drives has not yet been achieved. The only attempts in the past to compensate for kinematic error have been made in [8] and [17]. In [8], the kinematic error was approximated with a simple sinusoid in the following way:

$$\tilde{\theta} = A \sin 2\theta_m.$$

The higher frequency components in the error were neglected. Based on this approximation, for a given load trajectory $\theta_l(t)$, the trajectory to be traversed by the motor $\theta_m(t)$ was determined using (1). Next, the motor position was controlled to follow the trajectory $\theta_m(t)$, thereby partially compensating for the kinematic error when the output tracks the trajectory $\theta_l(t)$. This

scheme required prior knowledge of the error waveform, and also it did not account for the error sensitivity to different factors reported in [12] and mentioned above. This compensation can be considered open loop because no load side feedback is used. The active compensation approach of [17] differed from the approach of [8] in that in [17] disturbance is injected at the current controller input to compensate for the error. Before implementing this scheme, the disturbance injection signal had to be calibrated based on the kinematic error profile, for which the measurement of acceleration at the output is used. Thus, this scheme too required prior knowledge of the kinematic error in a different way and accomplished the compensation task in the open-loop sense. Additionally, once calibrated, the scheme does not promise complete compensation with changed assembly, loading and environmental conditions. Thus, both of these approaches seek to compensate for the error in an open-loop sense, using the stored information of the kinematic error.

In this paper, we propose control algorithms to completely compensate for kinematic error without using prior information of the error form. We first develop a mathematical model that represents nonlinear dynamic effects of kinematic error in harmonic drives. A general form of kinematic error is assumed while deriving the equations of motion of a drive using Lagrange formulation. Next, with reference to this model, nonlinear control algorithms are proposed to compensate completely for the kinematic error both in setpoint and trajectory tracking. The asymptotic stability of error dynamics equilibrium with the proposed controllers is demonstrated using Lyapunov theory. Furthermore, simulation and experimental results obtained using a dedicated harmonic drive test setup verify the effectiveness of these controllers. The proposed controllers achieve the compensation task independent of the form of kinematic error and no prior information regarding the form is necessary. The control scheme uses both load side and motor side feedback instead. Hence, it is a closed-loop approach as opposed to the open-loop approach (that uses only motor side feedback) used in [8] and [17]. Thus, our compensation approach differs distinctly from that of [8] and [17], the major difference being that we seek complete compensation irrespective of the error form using a closed-loop algorithm.

This paper is organized as follows. First, Section II presents the Lagrangian dynamic model of a dedicated harmonic drive test setup and then discusses the important model properties which are used later in the controller stability analysis. Section III presents a setpoint control algorithm along with the corresponding stability proof based on Lyapunov theory. Section IV presents a trajectory tracking control algorithm along with the stability proof. The results of simulations and experiments obtained with these algorithms are presented in Section V. This section also discusses various issues involved in the experimental implementation of the controllers. Finally, Section VI summarizes the results.

II. Dynamic Model of a Harmonic Drive Test Setup

This section presents a mathematical model of a dedicated harmonic drive test setup developed in [18] and used for the purpose of this work. In addition, the properties of this model that are important from a control perspective are presented. Since the focus of this work is kinematic error, it is represented in its most general form $\tilde{\theta} = \tilde{\theta}(\theta_m)$, and the flexibility and friction effects are neglected while deriving the equations governing the system dynamics. The experimental conditions are tailored to minimize excitation of flexibility and to avoid dynamic friction effects. In particular, the static friction effects are compensated for by using a Coulomb friction model, and unidirectional motion with slow speeds is maintained in all the experiments.

Fig. 3 shows a schematic diagram of the test setup that is depicted in Fig. 8 and described in Appendix I. The diagram shows all the parameters of the system, and Table I lists their values. These values are obtained experimentally using standard system identification techniques and are further verified using manufacturers' data. Note that the torque sensor shown in the figure is not used for the purpose of this work.

Considering the assumptions mentioned above, the kinetic energy T of the system and the Rayleigh function $\mathcal{F}$ for energy dissipation are given by

$$\begin{aligned} T &= \tfrac{1}{2} J_m \dot{\theta}_m^2 + \tfrac{1}{2} J_l \dot{\theta}_l^2 \\ \mathcal{F} &= \tfrac{1}{2} B_m \dot{\theta}_m^2 + \tfrac{1}{2} B_l \dot{\theta}_l^2. \end{aligned} \tag{2}$$

The two variables, motor position θ_m and load position θ_l in the equations above, are constrained by (1) which defines the kinematic error $\tilde{\theta} = \tilde{\theta}(\theta_m)$. Thus the system has only one degree of freedom, and it can be expressed in terms of either the motor variable θ_m or the load variable θ_l. By rearranging (1), we get

$$\theta_l = \frac{\theta_m}{N} - \tilde{\theta}. \tag{3}$$

Differentiating this equation with respect to time yields

$$\dot{\theta}_l = Y \dot{\theta}_m \tag{4}$$

where

$$Y = Y(\theta_m) = \frac{1}{N} - \frac{d\tilde{\theta}}{d\theta_m}. \tag{5}$$

The variable $Y(\theta_m)$ can be interpreted as a new gear transmission ratio which depends on the motor position θ_m due to the effects of kinematic error. Using relation (4) between motor velocity and load velocity, the kinetic energy T and the Rayleigh energy $\mathcal{F}$ can be represented either in terms of motor variables or in terms of load variables. Differentiating (5) with respect to time, we get

$$\dot{Y} = -\tilde{\theta}'' \dot{\theta}_m \tag{6}$$

where

$$\tilde{\theta}'' = -\frac{d}{d\theta_m}\left(\frac{d\tilde{\theta}}{d\theta_m}\right). \tag{7}$$

Representing T and $\mathcal{F}$ in terms of $\dot{\theta}_l$ for the Lagrange formulation with θ_l as an independent variable and using (5) and

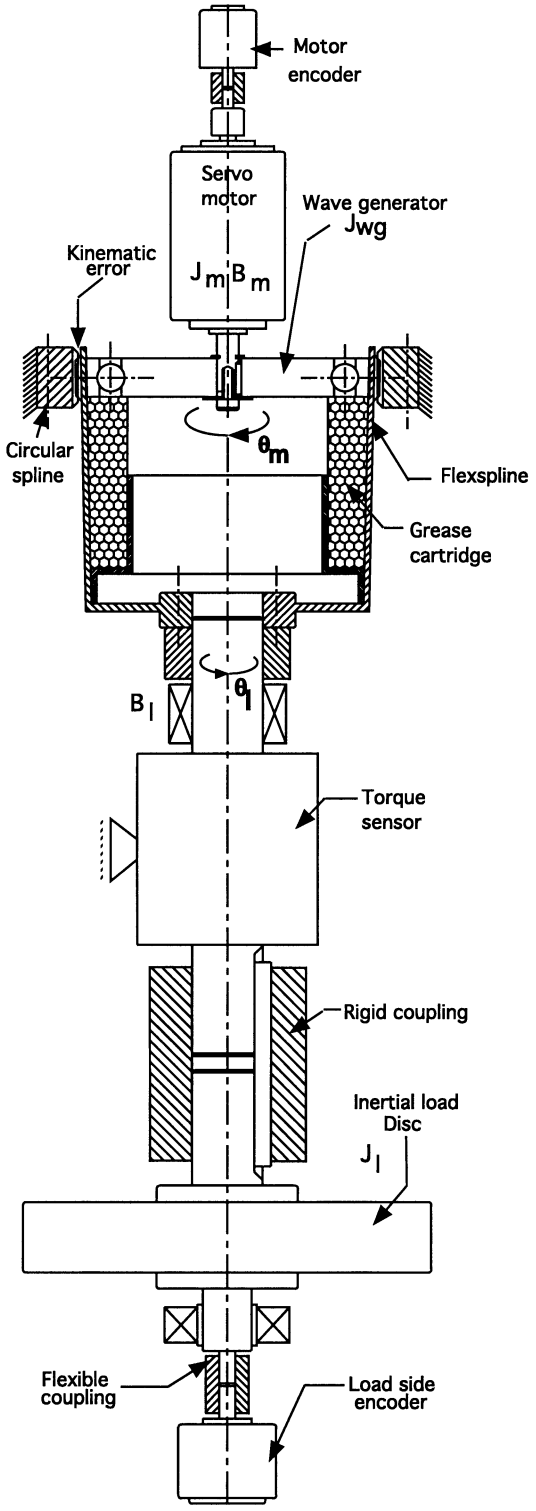

Fig. 3. Schematic diagram of harmonic drive test setup.

(6), we get a single second-order nonlinear differential equation governing the system dynamics in terms of load variables $(\theta_l, \dot{\theta}_l, \ddot{\theta}_l)$ as

$$\left(\frac{J_m}{Y^2}+J_l\right)\ddot{\theta}_l+\frac{J_m\tilde{\theta}''}{Y^4}\dot{\theta}_l^2+\left(\frac{B_m}{Y^2}+B_l\right)\dot{\theta}_l=\frac{\tau_m}{Y}. \quad (8)$$

TABLE I
SYSTEM PARAMETERS USED FOR SIMULATION

Parameter		Numerical Value
Inertia on Motor Side	J_m	$4.5\times10^{-4}kgm^2$
Inertia on Load Side	J_l	$5.0\times10^{-2}kgm^2$
Damping on Motor Side	B_m	$3.3\times10^{-3}Nm-s$
Damping on Load Side	B_l	$5.0\times10^{-4}Nm-s$
Gear Ratio	N	50

The nonlinearity in the system is represented in the nonlinear functions Y and $\tilde{\theta}''$. For convenience, we represent (8) in the standard form in the following way:

$$D\ddot{\theta}_l+C\dot{\theta}_l+B\dot{\theta}_l=\frac{\tau_m}{Y} \quad (9)$$

where

$$D=\frac{J_m}{Y^2}+J_l,\quad C=\frac{J_m\tilde{\theta}''}{Y^4}\dot{\theta}_l,\quad \text{and}\quad B=\frac{B_m}{Y^2}+B_l.$$

Note II.1: Representing T and $\mathcal{F}$ in terms of $\dot{\theta}_m$ for Lagrange formulation with θ_m as an independent variable, we get a similar second-order differential equation governing the same dynamics in terms of motor variables $(\theta_m, \dot{\theta}_m, \ddot{\theta}_m)$ as

$$(J_m+Y^2J_l)\ddot{\theta}_m-YJ_l\tilde{\theta}''\dot{\theta}_m^2+(B_m+Y^2B_l)\dot{\theta}_m=\tau_m. \quad (10)$$

We use (9) for the purpose of stability analysis presented in Sections III and IV, and the equivalent equation (10) for the purpose of simulation. From (9) we observe that when the quantity $Y(\theta_m)=0$, the system becomes singular. However, according to Property B.1 in Appendix II, $Y(\theta_m)$ is found to be always nonzero. Next, we state and prove the property of the dynamic model represented by (9).

Property II.1: With reference to (9), $\dot{D}-2C$ is zero.

Proof: By differentiating D with respect to time, we get

$$\dot{D}=\frac{-2J_m}{Y^3}\dot{Y}. \quad (11)$$

Now, from (4) and (6), it follows that

$$\dot{D}=\frac{2J_m\tilde{\theta}''}{Y^4}\dot{\theta}_l=2C. \quad (12)$$

■

This skew–symmetry property will be used later for the Lyapunov stability analysis of the controllers.

To carry out simulations using (9) or (10), we need the kinematic error profile $\tilde{\theta}(\theta_m)$ and its two successive derivatives with respect to θ_m. This requires that the discrete experimental data for $\tilde{\theta}$ be represented in a continuous and at least twice differentiable function of θ_m. This can be achieved, as shown in [12], by first representing the discrete data in the form of a piecewise continuous curve and then using a projection of this curve onto the finite-dimensional basis of Fourier eigenfunctions. In other words, we use the best approximation of the experimental profile in the subspace spanned by a finite number (in this case

16) of Fourier eigenfunctions. The profile is thus represented by [12]

$$\tilde{\theta} = \frac{a_0}{2} + \sum_{n=1}^{k} [a_n \cos(n\theta_m) + b_n \sin(n\theta_m)] \tag{13}$$

where

$$a_n = \frac{1}{\pi} \int_0^{2\pi} \tilde{\theta}(\theta_m) \cos(n\theta_m)\, d\theta_m$$

and

$$b_n = \frac{1}{\pi} \int_0^{2\pi} \tilde{\theta}(\theta_m) \sin(n\theta_m)\, d\theta_m. \tag{14}$$

The Fourier coefficients (a_n, b_n) are obtained by using numerical integration techniques and linear interpolation of the data.

In the next two sections, in order to achieve high precision positioning, we develop setpoint and trajectory tracking control strategies that compensate for the kinematic error.

III. Setpoint Control

Based on the model dynamics derived previously, this section develops a control law to compensate for kinematic error in setpoint control of load position. The asymptotic stability in compensation is proved using Lyapunov stability theory.

Let the setpoint control problem consist of driving the load shaft position θ_l to a constant reference position θ_l^r. Let both motor and load state feedback be available as shown in Fig. 4. Note that $\dot{\theta}_l^r$ and $\ddot{\theta}_l^r$ are zero since θ_l^r is constant. In this setting, we present in the following theorem, a setpoint control strategy to drive the load position θ_l to the reference position θ_l^r, thereby compensating completely for the kinematic error.

Theorem 1: In reference to the harmonic drive plant dynamics [(9) or (10)], let the control input τ_m be given by the following PD-type controller:

$$\tau_m = Y(\theta_m) \left(K_p \theta_l^e - K_d \dot{\theta}_l \right) \tag{15}$$

where K_p and K_d are positive constants, and θ_l^e is defined as $\theta_l^r - \theta_l$. Then the load will be driven to the reference position θ_l^r such that $(\theta_l^r - \theta_l) \to 0$ and $\dot{\theta}_l \to 0$ as $t \to \infty$, for all kinematic error profiles $\tilde{\theta}(\theta_m)$. ∎

Note that the control algorithm does not contain an acceleration term.

Proof: By substituting the control law given by (15) into (9), we get the following equation governing the error dynamics:

$$D\ddot{e}_l + C\dot{e}_l + (B + K_d)\dot{e}_l + K_p e_l = 0 \tag{16}$$

where $e_l = \theta_l - \theta_l^r$ defines the error in the load position

$$D = \frac{J_m}{Y^2} + J_l, \quad C = \frac{J_m \tilde{\theta}''}{Y^4}\, \dot{\theta}_l, \quad \text{and} \quad B = \frac{B_m}{Y^2} + B_l.$$

Note that since θ_l^r is constant, (16) represents an autonomous system.

Next, let us consider the energy-based function

$$V(e_l, \dot{e}_l) = \tfrac{1}{2} D \dot{e}_l^2 + \tfrac{1}{2} K_p e_l^2 \tag{17}$$

where the first term corresponds to the kinetic energy of the system and the second term accounts for the potential energy due to proportional feedback. Since $D > 0$, $K_p > 0$, and $V(0, 0) = 0$, $V(e_l, \dot{e}_l)$ is a positive definite function [19] and hence is a suitable Lyapunov function candidate. Now

$$\begin{aligned} \dot{V} &= \dot{e}_l[-C\dot{e}_l - (B + K_d)\dot{e}_l - K_p e_l] + \tfrac{1}{2}\dot{D}\dot{e}_l^2 + K_p e_l \dot{e}_l \\ &= -(B + K_d)\dot{e}_l^2 + \tfrac{1}{2}\left(\dot{D} - 2C\right)\dot{e}_l^2 \\ &= -(B + K_d)\dot{e}_l^2 \le 0 \end{aligned} \tag{18}$$

since B and K_d are both positive. It follows that the equilibrium $(e_l, \dot{e}_l) = (0, 0)$ is stable. Asymptotic stability follows by invoking LaSalle's theorem [19]. ∎

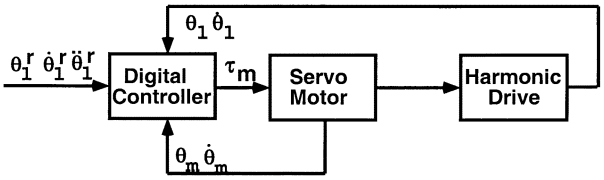

Fig. 4. Schematic diagram of the controller.

IV. Tracking Control

This section focuses on trajectory tracking with harmonic drives using a nonlinear control algorithm to compensate for kinematic error. We present a control strategy for tracking the load position along a desired trajectory and the corresponding stability proof. With this strategy, we prove, as in the case of setpoint control, that the tracking error asymptotically approaches zero irrespective of the profile of kinematic error.

Assume that the load position is to track a reference trajectory $\theta_l^r(t)$. Let $\theta_l^r(t)$ be a twice differentiable function of time t. Furthermore, let both motor and load state feedback be available (see Fig. 4). In this setting, we present the following trajectory tracking control algorithm.

Theorem 2: In reference to harmonic drive plant dynamics [see (9) or (10)], let the control input τ_m be given by the following controller:

$$\begin{aligned} \tau_m &= Y(\theta_m)[Da + Cv + Bv - K_d r], \\ e &= \theta_l - \theta_l^r \\ v &= \dot{\theta}_l^r - \Lambda e \\ r &= \dot{\theta}_l - v = \dot{e} + \Lambda e \\ a &= \dot{v} = \ddot{\theta}_l^r - \Lambda \dot{e} \end{aligned} \tag{19}$$

where K_d and Λ are positive constants. Then the load will be driven to follow the reference trajectory such that $(\theta_l^r(t) - \theta_l) \to 0$, and $(\dot{\theta}_l^r(t) - \dot{\theta}_l) \to 0$ as $t \to \infty$, for all kinematic error profiles $\tilde{\theta}(\theta_m)$. ∎

Proof: By substituting (19) into (9), we get the following equation in terms of the new error variable r:

$$D\dot{r} + (C + B)r + K_d r = 0 \tag{20}$$

where $r = \dot{e} + \Lambda e$. Note that (20) represents a nonautonomous system. Next, let us again consider a function

$$\begin{aligned} V(t, e, \dot{e}) &= \tfrac{1}{2} D r^2 + \Lambda K_d e^2 \\ &= \begin{bmatrix} e & \dot{e} \end{bmatrix} \begin{bmatrix} \frac{1}{2}D\Lambda^2 + \Lambda K_d & \frac{1}{2}D\Lambda \\ \frac{1}{2}D\Lambda & \frac{1}{2}D \end{bmatrix} \begin{bmatrix} e \\ \dot{e} \end{bmatrix}. \end{aligned} \tag{21}$$

Since $D > 0$ and bounded (see Property B.1 in Appendix II), Λ, $K_d > 0$ and $V(t, 0, 0) = 0$, $V(t, e, \dot{e})$ is positive definite and decrescent [19] and hence is a suitable Lyapunov function candidate. Differentiating V and making simplifications using (9) and Property II.1, we get

$$\begin{aligned}\dot{V} &= -(B + K_d)r^2 + 2\Lambda K_d e\dot{e} \\ &= -(B + K_d)\Lambda^2 e^2 - 2B\Lambda e\dot{e} - (B + K_d)\dot{e}^2 \\ &= -\begin{bmatrix} e & \dot{e} \end{bmatrix} \begin{bmatrix} (B + K_d)\Lambda^2 & B\Lambda \\ B\Lambda & (B + K_d) \end{bmatrix} \begin{bmatrix} e \\ \dot{e} \end{bmatrix}. \quad (22)\end{aligned}$$

Note that $\dot{V}(t, e, \dot{e}) < 0$ (negative definite), since B, K_d are both positive. Hence, equilibrium $(e, \dot{e}) = (0, 0)$ is asymptotically stable [19], and the controller achieves successful tracking irrespective of the profile of kinematic error. ■

V. Simulation and Experimental Results

The control algorithms developed in Sections III and IV are implemented in simulation using the ordinary differential equation solver in MATLAB [22]. The experimental implementation is carried out using our dedicated harmonic drive test setup of Fig. 8. This section presents the important issues in experimental implementation and the results of simulations and experiments.

A. Experimental Implementation

The experimental implementation of the control schemes presented in Sections III and IV does not require any prior information regarding the profile of the kinematic error $\tilde{\theta}$. All the required terms in the control law are computed online. This section deals with different issues involved in these computations.

Computation of Y: Digital implementation of Y can be realized using a causal approximation of derivative terms in (4). Thus, we have

$$Y = \frac{d\theta_l/dt}{d\theta_m/dt} = \frac{d\theta_l}{d\theta_m} \approx \frac{\Delta\theta_l}{\Delta\theta_m} \quad (23)$$

where the operator Δ represents the difference between the value of variable at a given sampling instant and that at a previous sampling instant. As $\Delta\theta_m \to 0$, (23) indicates a possible singularity. We carry out the following analysis to implement the computation devoid of singularity. The variational analysis of (1) shows that

$$d\tilde{\theta} = \frac{d\theta_m}{N} - d\theta_l. \quad (24)$$

By dividing the equation by $d\theta_m$, rearranging the terms, and taking limit as $d\theta_m \to 0$ on both the sides, we get

$$\lim_{d\theta_m \to 0} Y = \lim_{d\theta_m \to 0} \frac{d\theta_l}{d\theta_m} = \frac{1}{N} - \lim_{d\theta_m \to 0} \frac{d\tilde{\theta}}{d\theta_m}. \quad (25)$$

The term $d\tilde{\theta}/d\theta_m$ represents the slope of the kinematic error curve. As $d\theta_m \to 0$, this term tends to be constant at a given motor position θ_m. Hence as $d\theta_m \to 0$, it follows from equation (25) that Y tends to remain constant at whatever value it has at that position. This constant value can not be equal to $1/N$ as given in property B.1 (see Appendix II). With this understanding, the computation of Y is implemented devoid of singularity.

Another issue in computing Y is that the numerical approximation of a derivative induces unnecessary high-frequency components. To reduce these high-frequency components and to reduce further the error in computation of $\tilde{\theta}''$, Y is filtered using a suitable second-order low-pass filter.

Computation of $\tilde{\theta}''$: From (5), we can get $d\tilde{\theta}/d\theta_m$ as

$$\tilde{\theta}' = \frac{d\tilde{\theta}}{d\theta_m} = \frac{1}{N} - Y \quad (26)$$

where Y is computed as in the previous section. Next, we can represent $\tilde{\theta}''$ using a similar causal approximation of derivative as

$$\tilde{\theta}'' \approx \frac{\Delta\tilde{\theta}'}{\Delta\theta_m}. \quad (27)$$

We use this formula to compute the second derivative $\tilde{\theta}''$. Again, we may expect a singularity as $\Delta\theta_m \to 0$. As in the previous case, the singularity can be avoided by obtaining the value of $\tilde{\theta}''$ in the limiting case as $\Delta\theta_m \to 0$ or equivalently as $d\theta_m \to 0$. We know from the analysis in the previous case that $\tilde{\theta}' = d\tilde{\theta}/d\theta_m$ tends to be a constant as $d\theta_m \to 0$. Similarly, $\tilde{\theta}''$ which represents the slope of $\tilde{\theta}'$ curve tends to remain constant as $d\theta_m \to 0$. In this case again, to remove the high-frequency components induced by the approximation of derivative, the signal $\tilde{\theta}''$ is filtered using a second-order low-pass filter.

Compensation for Friction: The friction in the drive is not considered in the mathematical model. Hence, the experimental conditions are tailored to suit the model. We assume a static Coulomb friction model for compensation and maintain unidirectional motion to avoid dynamic friction effects. The control input is modified based on the Coulomb model used for compensating friction

$$u = \tau_m + F_f \quad (28)$$

where F_f represents the Coulomb friction term. This friction is identified based on simple experiments. To realize the unidirectional motion in the setpoint and trajectory tracking experiments, the gain parameters K_p and K_d are chosen to avoid overshoot. Also, in tracking experiments, the reference trajectory is chosen such that the reference velocity does not change sign, thereby ensuring the unidirectional motion.

B. Setpoint Control Results

Fig. 5 presents the simulation and experimental error history in implementing the setpoint control strategy. We observe that the load position error $(\theta_l - \theta_l^r)$ finally goes to zero in simulation and to a point within the encoder resolution in experiments. Thus, a successful compensation of kinematic error in setpoint control of harmonic drive is achieved as proposed. In the steady state, the observation of motor position error (computed as $\theta_m - \theta_l^r N$) shows a constant error which corresponds to the kinematic error at the final motor position. The final kinematic error can have different value in simulation and experiments. This is because the kinematic error profile used in simulation may differ from that in the experiments due to its de-

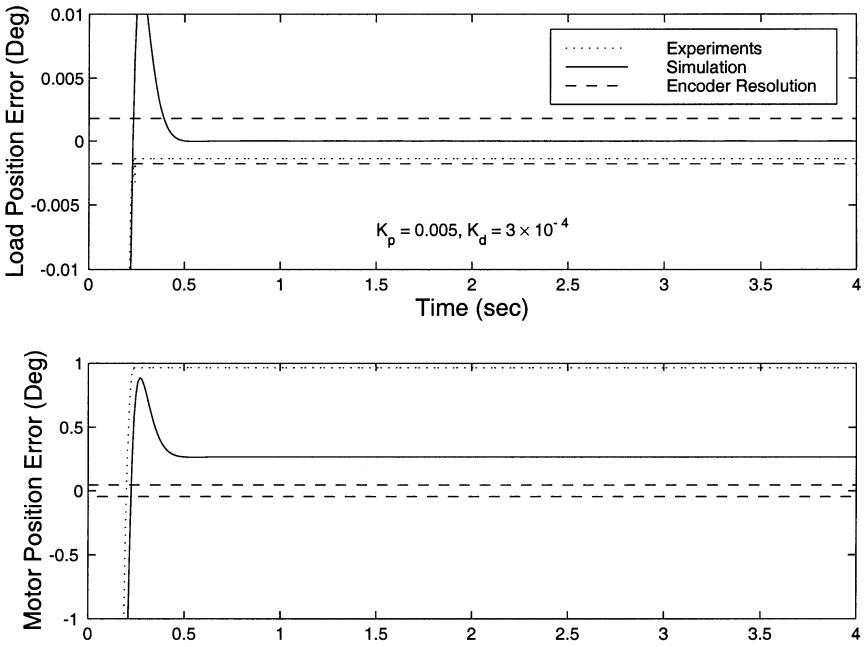

Fig. 5. Errors in setpoint control of the load position output of the harmonic drive where $\theta_l^r = 5°$.

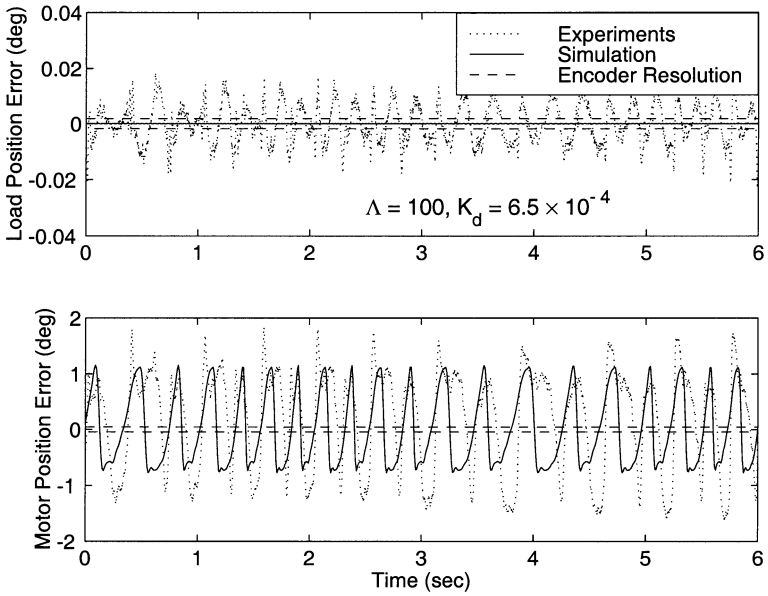

Fig. 6. Steady-state errors when load position tracks the trajectory $\theta_l^r(t) = 2\sin((\pi/2)t) + 12t$.

pendence on different factors mentioned already. Also, a phase lag between the two profiles can be another source of this difference. From the final shift in the motor position, we can conclude that the controller dynamically adjusts the motor position so as to make the load position error-free. In this way, the controller achieves complete compensation for the error. Close observation of the results shows that there is an overshoot in the results of simulation but not in those of experiments for the same gain values. This can be attributed to unmodeled dynamic friction effects which become dominant near zero velocities.

C. Tracking Control Results

Fig. 6 shows the simulation and experimental steady state results when the load position tracks a trajectory defined by $\theta_l^r(t) = 2\sin((\pi/2)t) + 12t$. The gain values used in tracking are also listed in the figure. Note that the trajectory is chosen to have a unidirectional motion to avoid dynamic friction effects and also lower velocities are used to minimize the unmodeled flexibility effects. We observe that the load position error again goes to zero in simulation and close to the limits on the resolution of encoder in experiments. Fig. 7 clearly distinguishes the tracking error from the kinematic error produced in the absence of the controller. The kinematic error profile shown in the figure is obtained in an open-loop experiment with constant torque input to the motor. Thus, reasonable tracking of load position is achieved within the experimental constraints. The small-amplitude high-frequency discrepancy in the experimental results can be attributed to unmodeled flexibility effects and the error

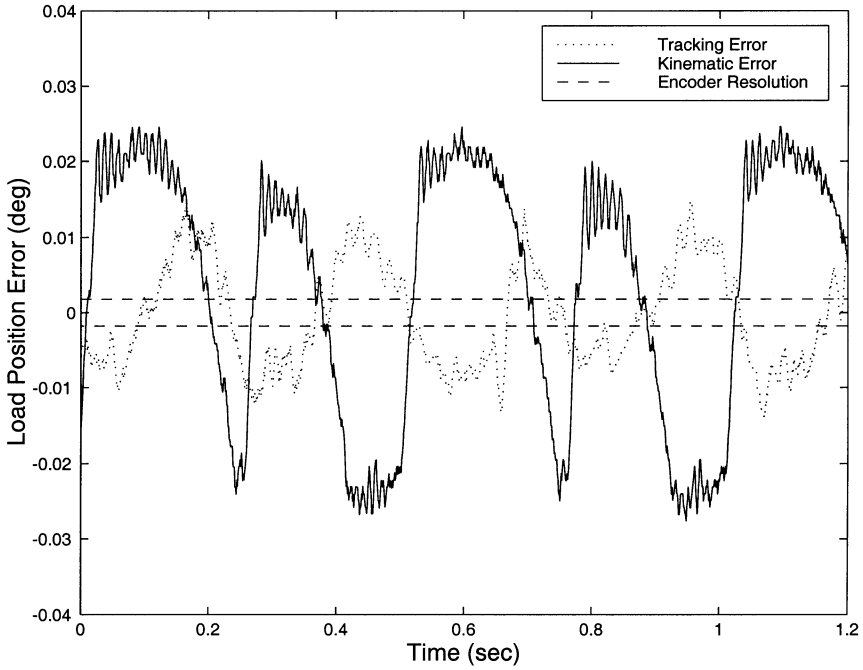

Fig. 7. Comparison of the steady-state tracking error and the kinematic error.

in the computation of numerical derivative $\tilde{\theta}''$. Also, Coulomb friction model which was assumed to represent the friction in the drive is not rich enough for the purpose of complete friction compensation. The motor position error profile in Fig. 6 shows the reflected kinematic error both in simulation and experiments. Thus, the tracking controller also adjusts the motor position dynamically so as to make the load position error-free. Complete modeling of the harmonic drive system considering flexibility and friction (hysteresis) is currently under study.

VI. Conclusion

This work presented nonlinear control algorithms for closed-loop compensation of kinematic error in setpoint and trajectory tracking with harmonic drives. Using Lyapunov stability theory, we proved that the steady-state error in the load position can be driven to zero with these algorithms. Furthermore, these algorithms do not require any information regarding the nonlinear, drive-specific kinematic error profile. Experimental and simulation results verify the effectiveness of these algorithms. Thus, these profile-independent algorithms can compensate for kinematic error in harmonic drives under varying operating conditions and, hence, would be very useful for precision control applications.

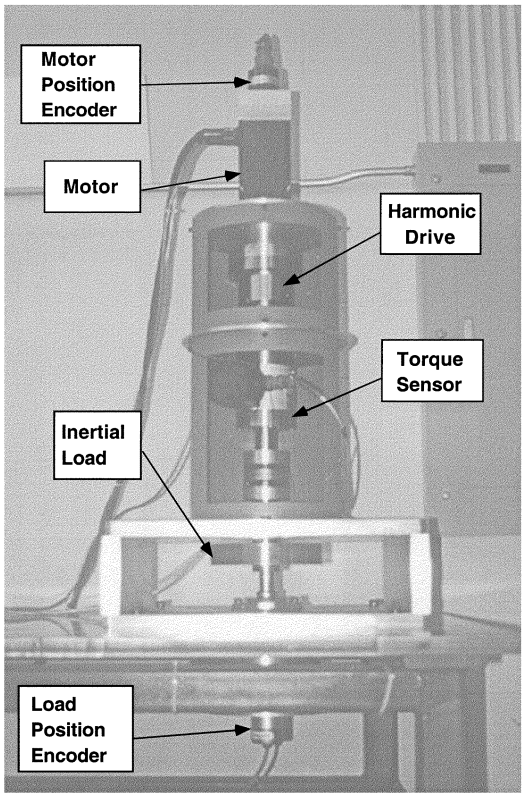

Fig. 8. View of the harmonic drive test apparatus.

Appendix I
Description of Harmonic Drive Test Apparatus

The dedicated apparatus for experimental examination of the nonlinearities in harmonic drives has been developed in [18] and is briefly described in this section. The system is composed of a servo motor, a harmonic drive (HDC-40 [2]) assembly module, and a digital control module. The digital control module has electromechanical interface with the assembly module to acquire system information using various sensors. In particular, the motor position is monitored by a rotary encoder (resolution $= 0.045^\circ$), the load position is measured by a laser rotary encoder (resolution $= 0.0018^\circ$), and the load torque is measured with a dc-operated noncontact rotating torque sensor (note that torque sensor is not used for the purpose of this work). Fig. 8

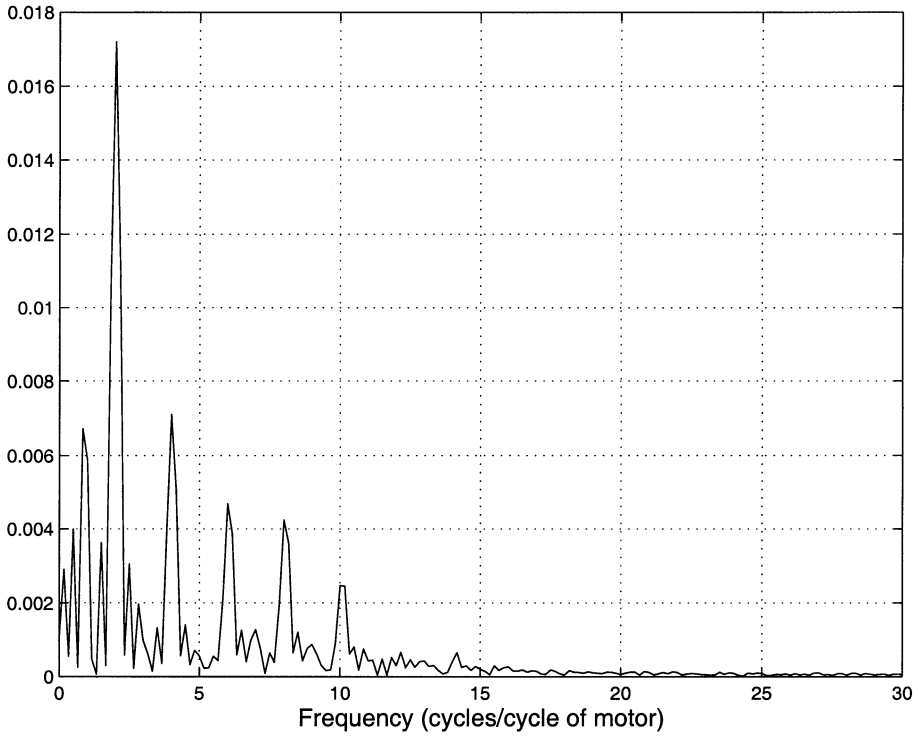

Fig. 9. Frequency response of kinematic error.

shows the photograph of the system. As can be seen, the system operates in the vertical plane.

APPENDIX II
PROPERTY OF KINEMATIC ERROR

Property B.1: The kinematic error in all harmonic drives is such that

1) $Y(\theta_m) > 0$ and is bounded for any θ_m;
2) $\tilde{\theta}''$ is bounded for any θ_m.

Discussion of Property B.1: For kinematic error in all harmonic drives, we claim that

$$\frac{1}{N} \gg \frac{d\tilde{\theta}}{d\theta_m}. \tag{29}$$

The claim is based on the nature of frequency response of kinematic error and the manufacturers' data regarding the kinematic error in harmonic drives. The frequency response of the kinematic error waveform, presented in Fig. 2, is shown in Fig. 9. We observe that the most significant contribution comes from the fundamental harmonic (twice the wave generator rotation θ_m) and that the higher harmonics decay at fast rate. Now, the fundamental component can be represented by $\tilde{\theta}_1 = \tilde{\theta}_{1\max} \sin 2\theta_m$. The maximum contribution of $\tilde{\theta}_1$ to the derivative $d\tilde{\theta}/d\theta_m$ is $2 \times \tilde{\theta}_{1\max}$. Similar contributions from higher terms would be $4 \times \tilde{\theta}_{2\max}$, $6 \times \tilde{\theta}_{3\max}$ and so on. Hence, with a conservative approximation, the maximum possible value of $d\tilde{\theta}/d\theta_m$ is given by

$$\left\| \frac{d\tilde{\theta}}{d\theta_m} \right\|_{\max} = 2 \times \tilde{\theta}_{1\max} + 4 \times \tilde{\theta}_{2\max} + 6 \times \tilde{\theta}_{3\max} + \cdots. \tag{30}$$

In (30), we observe that the coefficients 2, 4, 6, … multiplying the contribution due to different harmonics increase linearly; however, amplitudes $\tilde{\theta}_{1\max}$, $\tilde{\theta}_{2\max}$, $\tilde{\theta}_{3\max}$, … decrease much faster as observed in Fig. 9. Hence, we can consider the first six terms to be the most significant and approximate the sum as

$$\left\| \frac{d\tilde{\theta}}{d\theta_m} \right\|_{\max} \approx 6 \times 2\tilde{\theta}_{1\max}. \tag{31}$$

Again, considering a conservative approximation, we replace $\tilde{\theta}_{1\max}$ in (31) by amplitude of kinematic error $\tilde{\theta}_{\max}$ to get

$$\left\| \frac{d\tilde{\theta}}{d\theta_m} \right\|_{\max} \approx 6 \times 2\tilde{\theta}_{\max}. \tag{32}$$

Computation of this sum for different harmonic drives including the worst possible case shows that $1/N \gg d\tilde{\theta}/d\theta_m$. For example, in the case of the harmonic drive used in this research, $1/N = 0.02$ and $||d\tilde{\theta}/d\theta_m||_{\max} = 0.006$ for the worst possible conditions of loading and assembly. Thus $1/N$ is much larger than $d\tilde{\theta}/d\theta_m$. It is possible that the frequency distribution may differ slightly based on a specific drive, assembly, loading, and environmental conditions. However, considering the conservative approximations in getting (32) and the fact that $1/N$ is still almost 3.3 times higher than $||d\tilde{\theta}/d\theta_m||_{\max}$, there is ample room for variation. Hence, for all harmonic drives we can conclude that $Y > 0$. Also, since $\tilde{\theta}_{\max}$ is bounded for all existing harmonic drives, it follows immediately from equation (32) and (5) that Y is also bounded.

Following similar arguments we can represent $\tilde{\theta}'' = d^2\tilde{\theta}/d\theta_m$ as

$$\left\| \frac{d^2\tilde{\theta}}{d\theta_m} \right\|_{\max} = 2^2 \times \tilde{\theta}_{1\max} + 4^2 \times \tilde{\theta}_{2\max} + \cdots. \tag{33}$$

Again, since the high-frequency contributions decrease at a faster rate, we conclude boundedness of $\tilde{\theta}''$ for bounded kinematic error. ■

ACKNOWLEDGMENT

The authors acknowledge the effort of S. Hejney, who built the harmonic drive test apparatus, and M. Were, who performed preliminary work on kinematic error.

REFERENCES

[1] [Online]. Available: http://www.harmonic-drive.com/.
[2] *HDC Cup Component Gear Set Selection Guide*. Peabody, MA: Harmonic Drive Technologies, 1995.
[3] C. W. Musser, "Strain wave gearing," U.S. Patent 2 906 143, 1955.
[4] ——, "Breakthrough in mechanical drive design: The harmonic drive," in *Machine Design*. Boston, MA: Research Adviser for the United Shoe Machinery Corp., 1960, pp. 160–172.
[5] A. F. Emel'yanov *et al.*, "Calculation of the kinematic error of a harmonic gear transmission taking into account the compliance of elements," in *Sov. Eng. Res.*, vol. 3, 1983, pp. 7–10.
[6] L. Hsia, "The analysis and design of harmonic gear drives," in *Proc. 1988 IEEE Int. Conf. Syst., Man, Cybern.*, 1988, pp. 616–619.
[7] R. T. Ramson, "Positional error analysis of harmonic drive gearing," M.S. thesis, Clemson Univ., Clemson, SC, May 1988.
[8] T. W. Nye and R. P. Kraml, "Harmonic drive gear error: Characterization and compensation for precision pointing and tracking," in *Proc. 25th Aerospace Mechanics Symp.*, Pasadena, CA, 1991, pp. 237–252.
[9] T. D. Tuttle, "Understanding and modeling the behavior of a harmonic drive gear transmission," M.S. thesis, Massachusetts Inst. Technol., Cambridge, MA, May 1992.
[10] N. Kircanski, A. A. Goldenberg, and S. Jia, "An experimental study of nonlinear stiffness, hysteresis, and friction effects in robot joints with harmonic drives and torque sensors," in *Proc. 3rd Int. Symp. Experimental Robot.*, Oct. 1983, pp. 327–340.
[11] W. Seyfferth, A. J. Maghzal, and J. Angeles, "Nonlinear modeling and parameter identification of harmonic drive gear transmissions," in *Proc. 32nd IEEE Conf. Robot. Automat.*, 1995, pp. 3027–3032.
[12] F. Ghorbel, P. S. Gandhi, and F. Altpeter, "On the kinematic error in harmonic drive gears," *Trans. ASME, J. Mech. Design*, vol. 123, pp. 90–97, Mar. 2001.
[13] A. V. Klypin *et al.*, "Calculation of the kinematic error of a harmonic drive on a computer," in *Sov. Eng. Res.*, vol. 5, 1985, pp. 9–12.
[14] S. A. Shuvalov, "Calculation of harmonic drives with allowance for pliancy of links," *Russian Eng. J.*, vol. 54, no. 6, pp. 47–52, 1974.
[15] Yu. B. Sinkevich, "Effect of teeth on the rim rigidity of the flexible gear wheel of a harmonic drive," *Russian Eng. J.*, vol. 58, no. 7, pp. 19–22, 1978.
[16] T. D. Tuttle and W. P. Seering, "Kinematic error, compliance, and friction in a harmonic drive gear transmission," in *1993 ASME Design Tech. Conf. 19th Design Automat. Conf.*, Albuquerque, NM, 1993, pp. 319–324.
[17] H. K. Tonshoff and J. Kummetz, "Active compensation of kinematic errors in servo drives for machine tools and robots," in *Amer. Contr. Conf.*, San Diego, CA, June 1999.
[18] S. W. Hejny and F. Ghorbel, "Harmonic drive test apparatus for data acquisition and control," Dynamic Syst. Contr. Lab., Dept. Mech. Eng., Rice Univ., Houston, TX, Int. Rep. ATP96-2, May 1997.
[19] M. Vidyasagar, *Nonlinear Systems Analysis*. Englewood Cliffs, NJ: Prentice-Hall, 1993.
[20] R. Ortega and M. W. Spong, "Adaptive motion control of rigid robots: A tutorial," in *Proc. 27th Conf. Decision Contr.*, Austin, TX, Dec. 1988, pp. 1575–1584.
[21] J. E. Slotine and W. Li, "On the adaptive control of robot manipulators," *Int. J. Robot. Res.*, vol. 6, no. 3, pp. 49–59, 1987.
[22] *MATLAB User's Guide*. Natick, MA: The Mathworks Inc., 1998.
[23] V. M. Popov, *Hyperstability of Control Systems*. New York: Springer-Verlag, 1973.
[24] dSPACE Digital Signal Processing and Control Engineering GmbH, *DSP-CITeco LD31/LD31NET User's Guide*, 1993.
[25] OEM Motion Control Specialists, *ST1 Digital Motion Controller User's Manual 024.8080*. Sewickley, PA: Atlas Copco Controls, Inc., 1994.
[26] dSPACE Digital Signal Processing and Control Engineering GmbH, *TRACE for MS-Windows 3.1 User's Guide*, 1993.

Prasanna S. Gandhi (S'00–A'01) received the B.Eng. degree in mechanical engineering from the University of Bombay, Mumbai, India, in 1994 and the M.Tech. degree from the Indian Institute of Technology, Bombay, Mumbai, India, in 1996. He received the Ph.D. degree in mechanical engineering from Rice University, Houston, TX.

He was with the Research and Development Division of Larsen and Toubro, Ltd. He is presently a Visiting Faculty in Mechanical Engineering Department at the Indian Institute of Technology, Bombay. His areas of research interest include nonlinear dynamical systems and control and robotics.

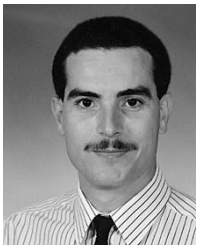

Fathi H. Ghorbel (S'86–M'87–SM'00) received the B.S. degree with honors from the Pennsylvania State University, University Park, in 1985, the M.S. degree from Carnegie-Mellon University, Pittsburgh, PA, in 1987, and the Ph.D. degree from the University of Illinois at Urbana-Champaign, Urbana, in 1991, all in mechanical engineering.

He is an Associate Professor at the Department of Mechanical Engineering and the Department of Bioengineering, Rice University, Houston, TX, where he is also the Director of the Dynamic Systems and Control Laboratory and the Robotics Laboratory, and Co-Director of the Biomedical Systems and Instrumentation Lab. His research is in the areas of systems and control theory, robotics, and biomedical engineering systems.

Dr. Ghorbel is a Member of the ASME, Sigma Xi, IFAC, SIAM, IASTED, and ASEE. He is the past Chair of the ASME Biomechanical Systems Panel, and the past Chair of the IEEE Control Systems Society's Technical Committee on Manufacturing Automation and Robotic Control. He is an Associate Editor for the IEEE TRANSACTIONS ON CONTROL SYSTEMS TECHNOLOGY, an Associate Editor for the ASME *Journal of Dynamic Systems, Measurement, and Control*, an Associate Editor for the IEEE Control Systems Society Conference Editorial Board, and a past Associate Editor for the *International Journal of Robotics and Automation*.